



On Normalized Least Mean Square Based Interference Cancellation Algorithm for Integrated Sensing and Communication Systems

YU Xiaohui, YU Shucheng, LIU Xiqing, PENG Mugen

(Beijing University of Posts and Telecommunications, Beijing 100876, China)

DOI: 10.12142/ZTECOM.202403004

<https://kns.cnki.net/kcms/detail/34.1294.TN.20240919.1205.004.html>, published online September 19, 2024

Manuscript received: 2024-08-04

Abstract: Integrated sensing and communication (ISAC) technology is a promising candidate for next-generation communication systems. However, severe co-site interference in existing ISAC systems limits the communication and sensing performance, posing significant challenges for ISAC interference management. In this work, we propose a novel interference management scheme based on the normalized least mean square (NLMS) algorithm, which mitigates the impact of co-site interference by reconstructing the interference from the local transmitter and canceling it from the received signal. Simulation results demonstrate that, compared to typical adaptive interference management schemes based on recursive least square (RLS) and stochastic gradient descent (SGD) algorithms, the proposed NLMS algorithm effectively cancels co-site interference and achieves a good balance between computational complexity and convergence performance.

Keywords: interference management; OFDM; 5G new radio; interference cancellation; radio frequency domain

Citation (Format 1): YU X H, YU S C, LIU X Q, et al. On normalized least mean square based interference cancellation algorithm for integrated sensing and communication systems [J]. *ZTE Communications*, 2024, 22(3): 21 – 28. DOI: 10.12142/ZTECOM.202403004

Citation (Format 2): X. H. Yu, S. C. Yu, X. Q. Liu, et al., “On normalized least mean square based interference cancellation algorithm for integrated sensing and communication systems,” *ZTE Communications*, vol. 22, no. 3, pp. 21 – 28, Sept. 2024. doi: 10.12142/ZTECOM.202403004.

1 Introduction

With the development of wireless communication technologies, the number of users and access devices is rapidly increasing, leading to an urgent shortage of communication spectrum resources. Traditionally, communication and sensing systems have been designed, developed and deployed independently. However, the congestion of the available radio spectrum has stimulated interest in combining communication and sensing functions within shared frequency bands and potentially on the same hardware platforms. In frequency bands below 10 GHz, such as the L-band (1 – 2 GHz), S-band (2 – 4 GHz), and C-band (4 – 8 GHz), radar systems, Long-Term Evolution (LTE), and wireless local area network (WLAN) communication systems are widely favored. Above 10 GHz, the operating frequencies of 5G millimeter-wave communication systems are very close to those of automotive millimeter-wave radars. Therefore, realiz-

ing integrated sensing and communication (ISAC) has become necessary and feasible^[1]. Currently, ISAC can be classified into two categories: One focuses on the coexistence of communication and sensing signals within the same frequency bands^[2]; the other aims to use a unified hardware platform with ISAC signals^[3].

Interference management is a critical challenge for the above ISAC implementation approaches. In coexistence-based ISAC systems, communication and sensing are implemented by independent hardware that transmits different signals. These systems are often not scheduled or synchronized with each other, resulting in severe mutual interference between communication and sensing signals. Consequently, dual-function radar-communication systems face high hardware complexity and difficulties in joint optimization of radar and communication functions. A current mainstream research direction is to design integrated waveforms based on existing communication signals to achieve communication and sensing simultaneously. In such ISAC systems, interference management becomes even more complex.

Many studies have focused on interference management in ISAC systems^[4], where opportunistic spectrum sharing^[5] and

This work were supported in part by the National Key Research and Development Program of China under Grant No. 2021YFB2900200, in part by National Natural Science Foundation of China under Grant Nos. 61925101 and 62271085, and in part by Beijing Natural Science Foundation under Grant No. L223007-2.

null space projection^[6] are the two typical methods for mitigating interference between communication and sensing signals. Recently, optimization theory has been widely investigated for its effectiveness in interference management in ISAC systems^[7-8]. The authors in Ref. [9] studied the spectrum sharing between multiple-input multiple-output (MIMO) based radar and communication systems in cluttered environments. To achieve effective clutter suppression, the ISAC system was designed by jointly optimizing the communication covariance matrix and the radar sub-sampling matrix. This scheme minimizes the interference power at the receiver of the radar system while maintaining the communication performance^[10]. In Ref. [11], a novel coexistence architecture for communication systems and pulse radars was proposed, together with a comprehensive performance evaluation. Different from the coordinated coexistence of communication and radar in most existing ISAC systems, the authors in Ref. [12] investigated the coexistence of communication and sensing functions in uncoordinated scenarios, with a particular focus on the dynamics of information sharing.

Additionally, interference cancellation in full-duplex systems has been a hot topic for long^[13]. An iterative successive nonlinear co-site interference cancellation method for in-band full-duplex communication was proposed in Ref. [14], which significantly improves co-site interference cancellation through multiple iterations. In Ref. [15], a low-latency precoding strategy for in-band full-duplex MIMO relay systems was introduced to achieve interference cancellation through time, space, and radio-frequency (RF) domains^[16]. The authors in Ref. [17] discussed joint analog and digital co-site interference cancellation techniques in full-duplex transceivers with frequency-dependent in-phase/quadrature (I/Q) imbalance. KIAYANI et al. studied adaptive nonlinear RF interference cancellation techniques to improve system isolation performance^[18]. In fact, interference management in ISAC systems is similar to that in full-duplex systems^[19]. Some works have designed dual-function radar and communication systems based on orthogonal frequency division multiplexing (OFDM) signals. In Ref. [20], monostatic sensing using OFDM in the presence of phase noise was investigated. The results show that with appropriate processing strategies, phase noise can not only be mitigated but also exploited to improve the sensing accuracy. In Ref. [21], the beam-domain full-duplex massive MIMO technology was investigated, where a precise beamforming scheme and a co-site interference cancellation strategy were proposed to improve spectrum utilization. LIU et al. proposed an effective channel estimation method for interference channel estimation in the coexistence of radar and communication systems^[22]. Moreover, the authors in Ref. [23] investigated integrating sensing capabilities into communication systems without significantly increasing system complexity.

In this work, we delve into interference management in

ISAC systems and propose a normalized least mean square (NLMS) algorithm to mitigate co-site interference. Specifically, we begin with a brief review of the widely implemented OFDM-based ISAC system models. Different from most existing works on ISAC technologies, we perform a detailed modeling and analysis of co-site interference in ISAC systems. On this basis, we propose the NLMS algorithm to reconstruct and cancel the co-site interference received from the local transmitter (Tx) at the integrated receiver (Rx). Simulation results demonstrate that the proposed algorithm effectively cancels interference and strikes a good balance between computational complexity and algorithm convergence performance. This work further advances the theory of ISAC interference management and has significant implications for guiding engineering practice.

2 System Model

Most existing works on ISAC have generally assumed that the signals received at the integrated receiver consist only of echoes and noise, neglecting the co-site interference caused by the local transmitter. To briefly illustrate the OFDM-based integrated signal processing, we first introduce the ideal interference-free ISAC system model. In this work, we investigate an OFDM-ISAC system with N subcarriers, where each subcarrier carries M OFDM symbols per frame. The subcarrier spacing is assumed to be Δf , and the symbol time can be obtained by $T = 1/\Delta f$. The transmitted OFDM symbol matrix is written as

$$\mathbf{F}_{\text{Tx}} = \begin{pmatrix} x_{0,0} & \cdots & x_{0,l} & \cdots & x_{0,M-1} \\ \vdots & \ddots & \vdots & \ddots & \vdots \\ x_{k,0} & \cdots & x_{k,l} & \cdots & x_{k,M-1} \\ \vdots & \ddots & \vdots & \ddots & \vdots \\ x_{N-1,0} & \cdots & x_{N-1,l} & \cdots & x_{N-1,M-1} \end{pmatrix}, \mathbf{F}_{\text{Tx}} \in \mathcal{A}^{N \times M} \quad (1)$$

The Doppler shift causes a phase shift in each element of \mathbf{F}_{Tx} , and each subcarrier experiences a different phase shift. For a delay of τ , the phase shift on the k -th subcarrier is expressed as $e^{j2\pi(k\Delta f + f_0)\tau}$, where f_0 is the carrier frequency. Hence, the echo signal of the l -th symbol on the k -th subcarrier is given as

$$(\mathbf{F}_{\text{Rx}})_{k,l} = b_0(\mathbf{F}_{\text{Tx}})_{k,l} \cdot \exp(j2\pi T f_D l - j2\pi\tau(k\Delta f + f_0)) + (\tilde{\mathbf{Z}})_{k,l} \quad (2)$$

where f_D is the Doppler shift and b_0 is the round-trip path loss. The matrix $\tilde{\mathbf{Z}} \in \mathbb{C}^{N \times M}$ represents the additive white Gaussian noise (AWGN) with power σ^2 . Clearly, \mathbf{F}_{Rx} contains the parameters τ, f_D and b_0 to be estimated. As \mathbf{F}_{Tx} is also known to the integrated receiver, the transmitted symbols are removed from the received echo signal by symbol-wise division as

$$(\mathbf{F})_{k,l} = \frac{(\mathbf{F}_{\text{Rx}})_{k,l}}{(\mathbf{F}_{\text{Tx}})_{k,l}} = b_0 \cdot \exp\left(j2\pi T f_D l - j2\pi\tau(k\Delta f + f_0)\right) + (\mathbf{Z})_{k,l}. \quad (3)$$

Here, $(\mathbf{Z})_{k,l} = (\tilde{\mathbf{Z}})_{k,l}/(\mathbf{F}_{\text{Tx}})_{k,l}$ is the noise sample after symbol-wise division. The Doppler shift f_D and the target distance R are obtained by discrete Fourier transform (DFT) for each row and inverse discrete Fourier transform (IDFT) for each column of $(\mathbf{F})_{k,l}$, respectively. Here, we denote the peak index of the n -th row of \mathbf{F} after DFT as $\tilde{m}_{F,n}$, and the speed of the target v can be obtained by

$$\tilde{m}_{F,n} = \lfloor f_D T M \rfloor, \quad v = \frac{f_D c}{2f_c}, \quad (4)$$

where $\lfloor \cdot \rfloor$ is the floor function, c is the light of speed, and f_c is the carrier frequency. Then, we denote the peak index of IDFT on the m -th column of \mathbf{F} as $\tilde{n}_{F,m}$, and the distance R between the sensing target and the base station is derived using^[24]

$$\tilde{n}_{F,m} = \left\lfloor \frac{2BR}{c} \right\rfloor, \quad (5)$$

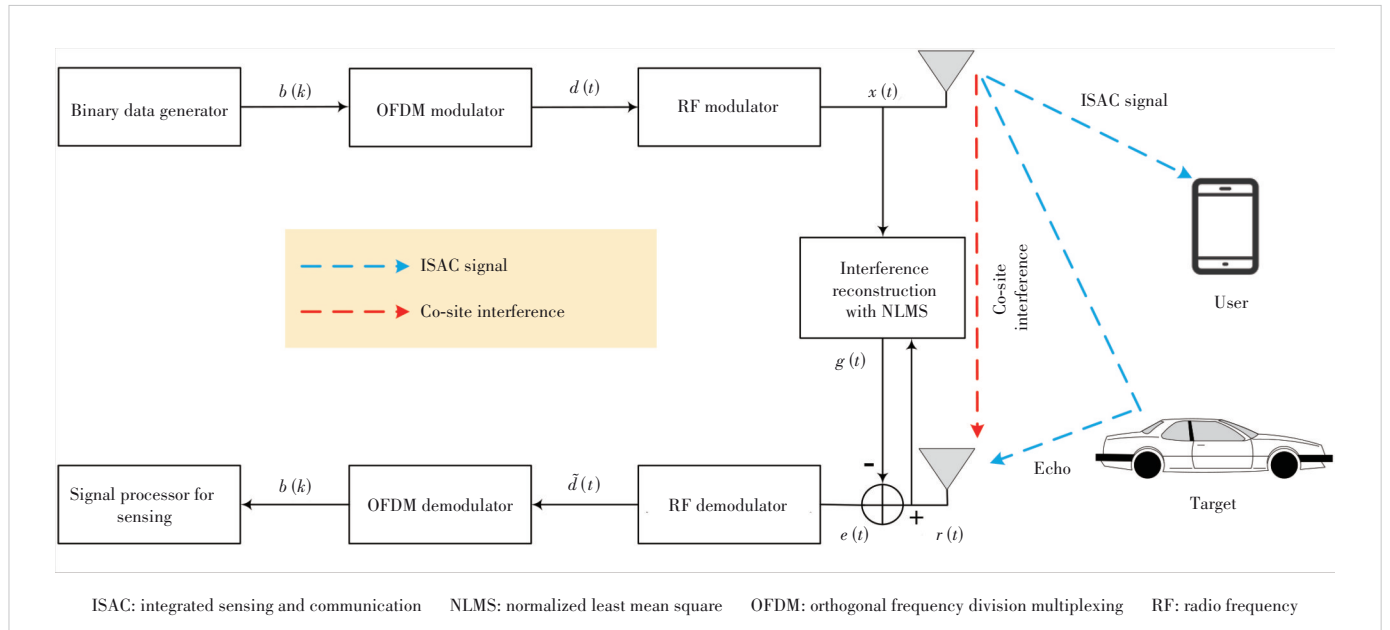
where B is the bandwidth of the ISAC signal.

Practically, the transmitted signals leaked from the local transmitter can cause significant co-site interference at the integrated receiver. To address this issue, we propose the NLMS algorithm with a decreasing convergence parameter. Fig. 1 il-

lustrates the ISAC system model with the proposed interference reconstruction and cancellation scheme. The NLMS algorithm reconstructs the co-site interference in the RF domain using a multi-tap circuit consisting of delayers, attenuators, and phase shifters. Interference cancellation is then performed at the receiver to eliminate the co-site interference. At the receiver of a communication user, the received signal undergoes RF demodulation, analog-to-digital conversion, cyclic prefix removal, and serial-to-parallel conversion. It is then transformed from the time domain to the frequency domain by the fast Fourier transform (FFT). Subsequently, we perform channel equalization, symbol decision, and symbol demapping on the frequency-domain signal to obtain the recovered communication data.

Next, we model the co-site interference received by the integrated receiver. As shown in Fig. 1, the Tx and Rx antennas are co-located, and mutual interference steps in the signal processing of the sensing receiver through the Tx-Rx channel. In this work, we term this mutual interference as the co-site interference, and the Tx-Rx channel can be modeled as a Rician fading channel^[25-27]. Thus, the co-site interference can be denoted as $\mathbf{Y}_{\text{ci}} = \mathbf{H} \cdot \mathbf{F}_{\text{Tx}}$. The channel matrix is written as

$$\mathbf{H} = \begin{bmatrix} h_0 & \cdots & h_0 \\ \vdots & & \vdots \\ h_k & \cdots & h_k \\ \vdots & & \vdots \\ h_{N-1} & \cdots & h_{N-1} \end{bmatrix}, \quad \mathbf{H} \in \mathcal{A}^{N \times M}, \quad (6)$$



▲ Figure 1. Schematic diagram of the ISAC system with interference reconstruction and cancellation

where the (k, l) -th element can be expressed as $h_k = \sqrt{r/(r+1)} h_k^{\text{los}} + \sqrt{1/(r+1)} h_k^{\text{nlos}}$, where r is the Rician factor. The terms h_k^{los} and h_k^{nlos} represent the line of sight (LoS) and non-LoS components, respectively. In a co-site interference channel, the LoS signal is relatively strong, resulting in a large value of r . Here, we express the received signal, including the echo signal, the co-site interference, and the noise, as

$$\begin{aligned} (\mathbf{F}_{\text{Rx}})_{k,l} &= b_0 (\mathbf{F}_{\text{Tx}})_{k,l} \cdot \exp(j2\pi T f_D l - j2\pi\tau(k\Delta f + f_0)) + \\ &h_k (\mathbf{F}_{\text{Tx}})_{k,l} \cdot \exp(-j2\pi\tau_{\text{SI}}(k\Delta f + f_0)) + (\tilde{\mathbf{Z}})_{k,l}, \end{aligned} \quad (7)$$

where τ_{SI} represents the co-site interference delay.

3 Normalized Least Mean Square Algorithm

A solution to cancelling the co-site interference is to establish a multi-tap circuit between the transmitter and receiver. Based on the known transmitted signal, the signal's amplitude and phase parameters are changed through the multi-tap circuit. Fig. 2 depicts the signal processing of the multi-tap circuit. The input signal $x(t)$ from the RF modulator can be expressed as

$$x(t) = \sqrt{2P} d(t) \cos(2\pi f_c t + \phi), \quad (8)$$

where P denotes the power of the transmitted signal, ϕ is the initial phase of the carrier, and $d(t)$ is the signal generated by the OFDM modulator. For simplicity, we assume that the signal power and the initial phase satisfy $P = 1/2$ and $\phi = 0$, and

then we have $x(t) = d(t) \cos(2\pi f_c t)$. Next, $x(t)$ goes through the delayer, attenuator, and phase shifter. The output signal of the l -th tap in the i -th iteration, denoted by $g_l^{(i)}(t)$, can be obtained as

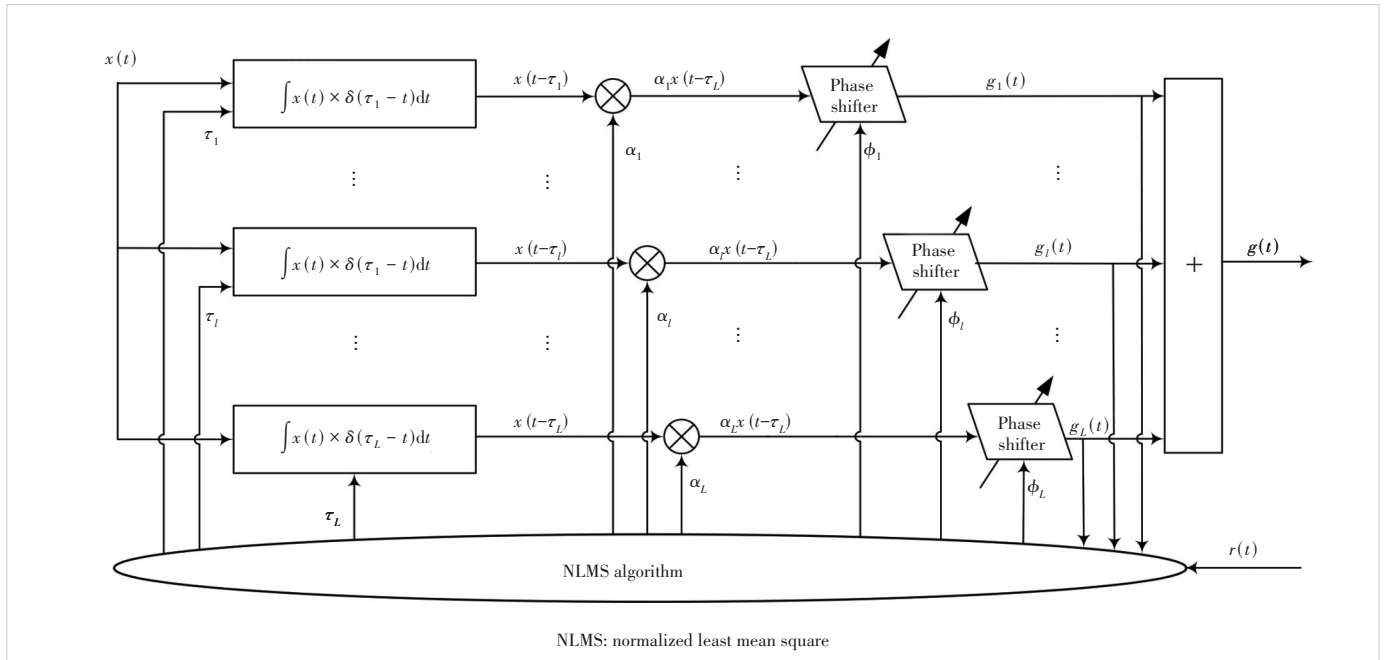
$$g_l^{(i)}(t) \triangleq \alpha_l^{(i)} x(t - \tau_l^{(i)}) e^{j\phi_l^{(i)}}, \quad i = 1, 2, \dots, I, \quad (9)$$

where $\alpha_l^{(i)}$, $\tau_l^{(i)}$ and $\phi_l^{(i)}$ are the attenuation component, delay and phase shift of the l -th path at the i -th iteration, respectively. The output signals of L paths undergo an adder to get the reconstructed interference signal $g(t)$. Then, by subtracting it from the received signal, the co-site interference cancellation is achieved. Within a time-frequency resource block, the complex amplitude of the signal can be approximated as a constant and the received signal can be simplified as

$$r(t) = b_0 x(t - \tau) \exp(j2\pi f_D t) + b_1 x(t - \tau_{\text{SI}}) + w(t), \quad (10)$$

where b_1 is the complex amplitude of the co-site interference. The first term in Eq. (10) is the sensing signal reflected by the target and the second term is the co-site interference. It is worth mentioning that the value of b_1 is much larger than b_0 , since b_0 refers to the round-trip path loss, which is proportional to the square of the distance between the transmitter and receiver. For the l -th tap, the error signal $e_l^{(i)}(t)$ and cost function $J_l^{(i)}(t)$ are defined respectively as

$$e_l^{(i)}(t) \triangleq r(t) - g_l^{(i)}(t), \quad (11)$$



▲ Figure 2. Interference reconstruction with NLMS

$$J_l^{(i)}(t) \triangleq \mathbb{E} \left[\left(e_l^{(i)}(t) \right)^2 \right] = \mathbb{E} \left[\left(r(t) - g_l^{(i)}(t) \right)^2 \right]. \quad (12)$$

In the traditional least mean square (LMS) algorithm^[28], the reconstructed interference signal $g_l^{(i+1)}(t)$ is updated by

$$g_l^{(i+1)}(t) = g_l^{(i)}(t) - \frac{1}{2} \mu \nabla J_l^{(i)}(t) = g_l^{(i)}(t) + \mu e_l^{(i)}(t) x(t), \quad (13)$$

where μ is the step size factor.

Specifically, the LMS algorithm uses a stochastic gradient descent (SGD) algorithm to update $g_l^{(i+1)}(t)$. At each adaptation moment, the gradient of the cost function is calculated from the difference between the reconstructed and real interference signals and multiplied by an appropriate step size factor μ . It is worth mentioning that when $x(t)$ is large, the LMS algorithm suffers from a problem of gradient noise amplification. To overcome this difficulty and achieve a balance between convergence speed and steady-state error, the updated equation in the proposed RF interference cancellation algorithm is

$$g_l^{(i+1)}(t) = g_l^{(i)}(t) + \left[\frac{\mu}{\rho + x^2(t)} \right] e_l^{(i)}(t) x(t), \quad (14)$$

where ρ is a very small value, preventing the denominator from being zero. By introducing $\tilde{\mu}(t) = \mu / [\rho + x^2(t)]$, we can view NLMS as a variable step-size algorithm. Small $x^2(t)$ results in large $\tilde{\mu}(t)$, accelerating the convergence for the NLMS algorithm. Conversely, large $x^2(t)$ and small $\tilde{\mu}(t)$ can avoid instability and divergence. Thus, by adaptively selecting an appropriate step size, NLMS can improve the robustness across different input signals.

4 Simulation Results and Discussions

In this section, we conduct simulations to verify the interference cancellation capability of the proposed NLMS algorithm and compare it with mainstream algorithms such as SGD and recursive least squares (RLS). In the simulation experiments, quadrature phase shift keying (QPSK) and 16-quadrature amplitude modulation (16 QAM) are used for modulation. The channel models include extended pedestrian A (EPA), extended typical urban (ETU), and extended vehicular A (EVA), with minimum mean square error (MMSE) employed for channel equalization. The rest of the simulation parameters are listed in Table 1.

The core idea of the RLS algorithm is to recursively update the filter parameters to make the output signal as close to the desired signal as possible. The forgetting factor λ determines the weight of new and old data during iterations. A higher forgetting factor gives more weight to new data, allowing the algorithm to track rapidly changing system parameters, while a

lower forgetting factor is suitable for systems with slowly varying parameters. The SGD algorithm uses gradient descent to update the filter weights, minimizing the mean squared error between the desired and actual signals. The SGD algorithm exhibits the lowest computational complexity among the three algorithms, followed by the NLMS and RLS algorithms. Given an L -tap circuit, the computational complexities of SGD and NLMS are $\mathcal{O}(L)$, while the complexity for RLS is up to $\mathcal{O}(L^2)$. Table 2 shows a detailed analysis of the computational complexities with respect to the three algorithms mentioned.

Fig. 3 plots the interference estimation error (IEE) versus the number of iterations for different algorithms, where the signal-to-interference ratio (SIR) is assumed to be -60 dB and the maximum number of iterations I is set to 1 000. The RLS algorithm with $\lambda = 0.99$ demonstrates the most excellent interference reconstruction capability, followed by the proposed NLMS algorithm. The SGD with $\mu = 0.1$ exhibits the worst interference reconstruction capability. In the SGD algorithm, a tradeoff can be observed between the convergence speed and the IEE. A large step size factor μ accelerates convergence but leads to a higher IEE, since SGD may miss the optimal solution in each update. To reduce the IEE, we can select a small step size, which however consumes much longer time.

▼Table 1. Simulation parameters

Parameter	Value
Rician factor	13 dB
Channel taps	10
Modulation	QPSK, 16 QAM
Subcarrier space (Δf)	30 kHz
FFT length	512
Communication channel type	EPA, ETU, EVA
Equalizer	MMSE
SIR	-60 dB
SGD step size (μ)	0.01, 0.1
RLS forgetting factor (λ)	0.99, 0.9
NLMS small value (ρ)	0.001

16 QAM: 16-quadrature amplitude modulation

EPA: extended pedestrian A

ETU: extended typical urban

EVA: extended vehicular A

FFT: fast Fourier transform

MMSE: minimum mean square error

NLMS: normalized least mean square

QPSK: quadrature phase shift keying

RLS: recursive least squares

SGD: stochastic gradient descent

SIR: signal-to-interference ratio

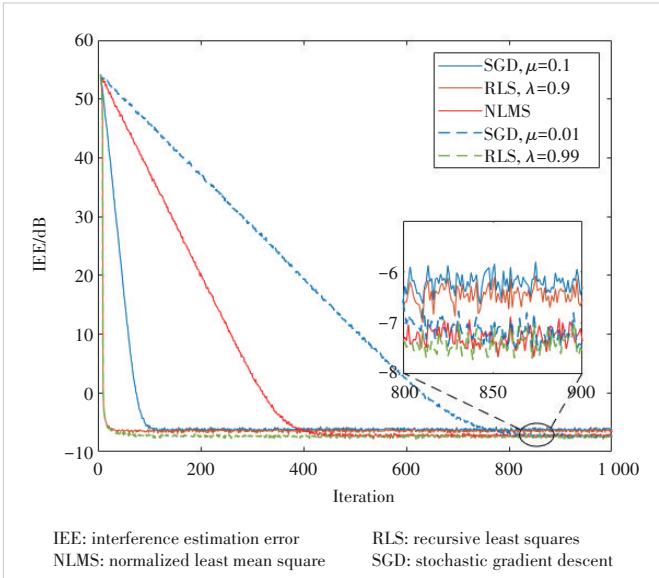
▼Table 2. Computational complexity of SGD, NLMS, and RLS algorithm^[29]

Algorithm	Number of Additions per Iteration	Number of Multiplications per Iteration
SGD	$L + 1$	$2L$
NLMS	$2L + 1$	$3L + 50$
RLS	$L^2 + L$	$2L^2 + 3L + 50$

NLMS: normalized least mean square

RLS: recursive least squares

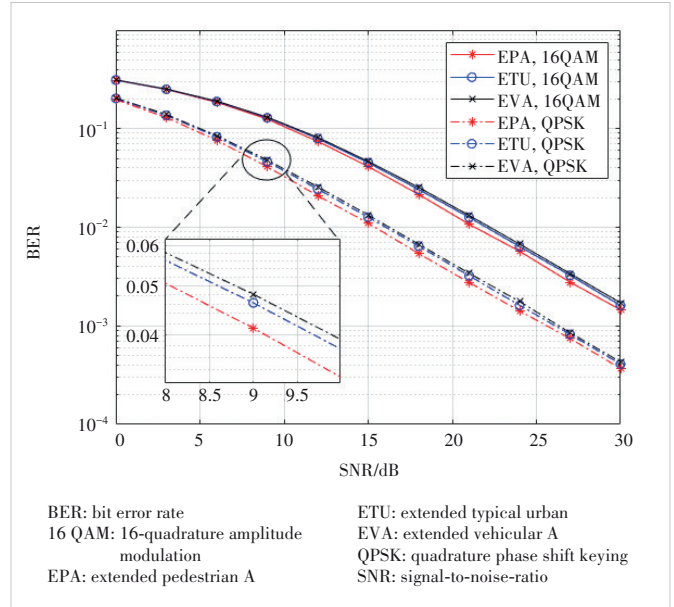
SGD: stochastic gradient descent



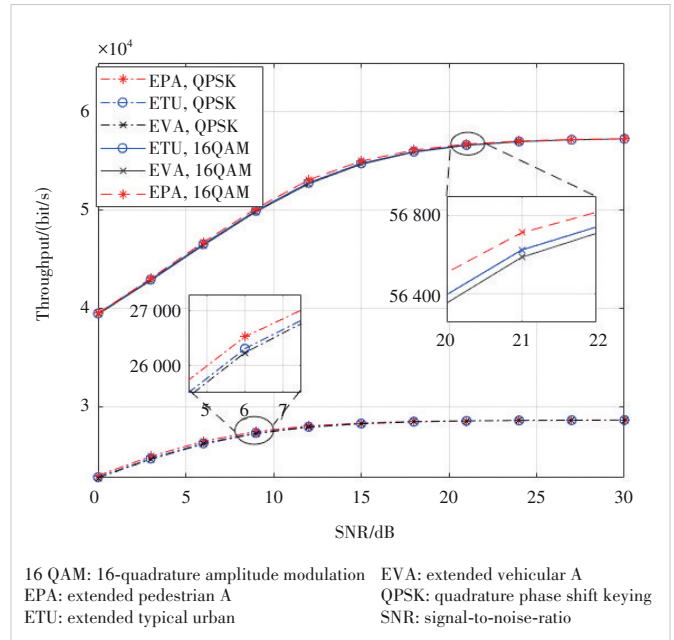
▲ Figure 3. IEEs of SGD, RLS and NLMS, with signal-to-interference ratio (SIR)=-60 dB

The SGD algorithm with $\mu = 0.1$ converges to an IEE of around -6 dB after 120 iterations. When the step size is reduced to 0.01, the SGD algorithm achieves a lower IEE of -7 dB at the cost of a slower convergence speed, i.e., 780 iterations. The NLMS can better handle this tradeoff and halves the iteration time. For the RLS algorithm, setting the forgetting factor to $\lambda = 0.99$ allows for more accurate interference reconstruction, yielding the lowest IEE. However, it does so at the cost of the greatly increased computational complexity $\mathcal{O}(L^2)$. In contrast, the proposed NLMS algorithm provides comparable interference reconstruction capability while keeping a low computational complexity $\mathcal{O}(L)$.

Next, we simulate the bit error rate (BER) and throughput of the ISAC system with the proposed NLMS algorithm under different modulation types and channels to evaluate its communication performance. As shown in Fig. 4, the BER of the ISAC system gradually decreases with increasing SNR. The EPA channel, with fewer multi-paths and lower average power attenuation per path compared to the ETU and EVA channels, results in the lowest BER. Compared to QPSK, the higher modulation order of QAM means that symbols are placed closer to each other in the constellation diagram, making the communication signal more sensitive to noise and resulting in a higher BER at the same SNR. Additionally, we present the throughput simulation results under different channel models and modulation types in Fig. 5. It can be observed that the ISAC system exhibits similar throughput across different channel models, with EPA and EVA yielding the highest and lowest throughput, respectively. Furthermore, 16 QAM achieves higher throughput than QPSK due to its higher modulation order.



▲ Figure 4. BER versus SNR under EPA, ETU, EVA channels, with two modulation types: QPSK and 16 QAM



▲ Figure 5. Throughput versus SNR under EPA, ETU, EVA channels, with two modulation types: QPSK and 16QAM

5 Conclusions and Future Work

In this work, we investigate the co-site interference problem in 5G NR ISAC systems. We model an OFDM-based ISAC system and provide a detailed overview of the corresponding ISAC signal processing flow. By modeling and analyzing the co-site interference in a single BS ISAC scenario, we propose an RF domain interference cancellation algorithm called the NLMS algorithm. By substituting μ for $\tilde{\mu}(t) = \mu / [\rho + x^2(t)]$,

the NLMS algorithm could adaptively adjust the step size factor, accelerating the convergence at a low cost of computing. Simulation results and analysis demonstrate that the NLMS algorithm could effectively cancel RF domain co-site interference. It also achieves a good balance among the iterations required for convergence, the computational complexity, and the capability of interference reconstruction. Compared to the RLS algorithm, the NLMS algorithm demonstrates similar interference reconstruction capability while maintaining a lower computational complexity $\mathcal{O}(L)$. In comparison to the SGD algorithm, it can better handle the tradeoff between the convergence speed and the IEE. Thus, the NLMS algorithm is a promising solution to co-site interference cancellation in ISAC systems. Our future work will focus on the joint design of more advanced interference cancellation algorithms in both the RF domain and baseband domain.

References

- [1] BAQUERO BARNETO C, RIIHONEN T, TURUNEN M, et al. Full-duplex OFDM radar with LTE and 5G NR waveforms: challenges, solutions, and measurements [J]. *IEEE transactions on microwave theory and techniques*, 2019, 67(10): 4042 – 4054. DOI: 10.1109/TMTT.2019.2930510
- [2] ZHENG L, LOPS M, ELДАР Y C, et al. Radar and communication coexistence: an overview: a review of recent methods [J]. *IEEE signal processing magazine*, 2019, 36(5): 85 – 99. DOI: 10.1109/MSP.2019.2907329
- [3] LIU F, CUI Y H, MASOUIROS C, et al. Integrated sensing and communications: toward dual-functional wireless networks for 6G and beyond [J]. *IEEE journal on selected areas in communications*, 2022, 40(6): 1728 – 1767. DOI: 10.1109/JSAC.2022.3156632
- [4] CHEN S J, CHENG R S. Clustering for interference alignment in multiuser interference network [J]. *IEEE transactions on vehicular technology*, 2014, 63(6): 2613 – 2624. DOI: 10.1109/TVT.2013.2292897
- [5] HONG B Q, WANG W Q, LIU C C. Interference utilization for spectrum sharing radar-communication systems [J]. *IEEE transactions on vehicular technology*, 2021, 70(8): 8304 – 8308. DOI: 10.1109/TVT.2021.3092410
- [6] BABAEL A, TRANTER W H, BOSE T. A nullspace-based precoder with subspace expansion for radar/communications coexistence [C]//Proc. IEEE Global Communications Conference (GLOBECOM). IEEE, 2013: 3487 – 3492. DOI: 10.1109/GLOCOM.2013.6831613
- [7] MAHAL J A, KHAWAR A, ABDELHADI A, et al. Spectral coexistence of MIMO radar and MIMO cellular system [J]. *IEEE transactions on aerospace and electronic systems*, 2017, 53(2): 655 – 668. DOI: 10.1109/TAES.2017.2651698
- [8] CADAMBE V R, ALI JAFAR S. Interference alignment and degrees of freedom of the K-user interference channel [J]. *IEEE transactions on information theory*, 2008, 54(8): 3425 – 3441. DOI: 10.1109/TIT.2008.926344
- [9] LI B, PETROPULU A P. Joint transmit designs for coexistence of MIMO wireless communications and sparse sensing radars in clutter [J]. *IEEE transactions on aerospace and electronic systems*, 2017, 53(6): 2846 – 2864. DOI: 10.1109/TAES.2017.2717518
- [10] QIAN J H, HE Z S, HUANG N, et al. Transmit designs for spectral coexistence of MIMO radar and MIMO communication systems [J]. *IEEE transactions on circuits and systems II: express briefs*, 2018, 65(12): 2072 – 2076. DOI: 10.1109/TCSII.2018.2822845
- [11] CHENG Z Y, LIAO B, SHI S N, et al. Co-design for overlaid MIMO radar and downlink MISO communication systems via Cramér-Rao bound minimization [J]. *IEEE transactions on signal processing*, 2019, 67(24): 6227 – 6240. DOI: 10.1109/TSP.2019.2952048
- [12] ZHENG L, LOPS M, WANG X D, et al. Joint design of overlaid communication systems and pulsed radars [J]. *IEEE transactions on signal processing*, 2018, 66(1): 139 – 154. DOI: 10.1109/TSP.2017.2755603
- [13] TUYEN LE A, HUANG X J, DING C, et al. An in-band full-duplex prototype with joint self-interference cancellation in antenna, analog, and digital domains [J]. *IEEE transactions on microwave theory and techniques*, 2024, 72(9): 5540 – 5549. DOI: 10.1109/TMTT.2024.3364113
- [14] HONG Z H, ZHANG L, WU Y Y, et al. Iterative successive nonlinear self-interference cancellation for In-band full-duplex communications [J]. *IEEE transactions on broadcasting*, 2024, 70(1): 2 – 13. DOI: 10.1109/TBC.2023.3291136
- [15] MALAYTER J R, LOVE D J. A low-latency precoding strategy for In-band full-duplex MIMO relay systems [J]. *IEEE transactions on wireless communications*, 2024, 23(3): 1899 – 1912. DOI: 10.1109/TWC.2023.3292985
- [16] HONG Z H, ZHANG L, LI W, et al. Frequency-domain RF self-interference cancellation for in-band full-duplex communications [J]. *IEEE transactions on wireless communications*, 2023, 22(4): 2352 – 2363. DOI: 10.1109/TWC.2022.3211196
- [17] HUANG X J, TUYEN LE A, GUO Y J. Joint analog and digital self-interference cancellation for full duplex transceiver with frequency-dependent I/Q imbalance [J]. *IEEE transactions on wireless communications*, 2023, 22(4): 2364 – 2378. DOI: 10.1109/TWC.2022.3211316
- [18] KIAYANI A, WAHEED M Z, ANTTILA L, et al. Adaptive nonlinear RF cancellation for improved isolation in simultaneous transmit – receive systems [J]. *IEEE transactions on microwave theory and techniques*, 2018, 66(5): 2299 – 2312. DOI: 10.1109/TMTT.2017.2786729
- [19] STURM C, WIESBECK W. Waveform design and signal processing aspects for fusion of wireless communications and radar sensing [J]. *Proceedings of the IEEE*, 2011, 99(7): 1236 – 1259. DOI: 10.1109/JPROC.2011.2131110
- [20] KESKIN M F, WYMEERSCH H, KOIVUNEN V. Monostatic sensing with OFDM under phase noise: From mitigation to exploitation [J]. *IEEE transactions on signal processing*, 2023, 71: 1363 – 1378. DOI: 10.1109/TSP.2023.3266976
- [21] XIA X C, XU K, ZHANG D M, et al. Beam-domain full-duplex massive MIMO: realizing co-time co-frequency uplink and downlink transmission in the cellular system [J]. *IEEE transactions on vehicular technology*, 2017, 66(10): 8845 – 8862. DOI: 10.1109/TVT.2017.2698160
- [22] LIU F, GARCIA-RODRIGUEZ A, MASOUIROS C, et al. Interfering channel estimation for radar and communication coexistence [C]//Proc. IEEE 20th International Workshop on Signal Processing Advances in Wireless Communications (SPAWC). IEEE, 2019: 1 – 5. DOI: 10.1109/SPAWC.2019.8815575
- [23] WU K, ZHANG J A, HUANG X J, et al. Integrating low-complexity and flexible sensing into communication systems [J]. *IEEE journal on selected areas in communications*, 2022, 40(6): 1873 – 1889. DOI: 10.1109/JSAC.2022.3156649
- [24] WEI Z Q, QU H Y, WANG Y, et al. Integrated sensing and communication signals toward 5G-A and 6G: a survey [J]. *IEEE Internet of Things journal*, 2023, 10(13): 11068 – 11092. DOI: 10.1109/JIOT.2023.3235618
- [25] LUO Y J, BI L H, ZHAO D. Adaptive digital self-interference cancellation based on fractional order LMS in LFM CW radar [J]. *Journal of systems engineering and electronics*, 2021, 32(3): 573 – 583. DOI: 10.23919/JSEE.2021.000049
- [26] QUAN X, LIU Y, PAN W S, et al. A two-stage analog cancellation architecture for self-interference suppression in full-duplex communications [C]//Proc. IEEE MTT-S International Microwave Symposium (IMS). IEEE, 2017: 1169 – 1172. DOI: 10.1109/MWSYM.2017.8058808
- [27] DOTY J M, JACKSON R W, GOECKEL D L. Analog cancellation of a known remote interference: Hardware realization and analysis [J]. *IEEE wireless communications letters*, 2024, 13(3): 829 – 833. DOI: 10.1109/LWC.2023.3346290

- [28] HAYKIN S. Adaptive Filter Theory (5th Ed.)[M]. Upper Saddle River, USA: Prentice Hall, 2014.
- [29] CIOLINO S. On the use of wavelet packets in ultra wideband pulse shape modulation systems [J]. IEICE transactions on fundamentals of electronics, communications and computer sciences, 2005, E88-A(9): 2310 – 2317. DOI: 10.1093/ietfec/e88-a.9.2310

Biographies

YU Xiaohui received his BS degree from the School of Information Engineering, Guangdong University of Technology, China in 2023. He is currently working toward an MS degree at Beijing University of Posts and Telecommunications, China. His research interests include integrated sensing and communication, and wireless communication.

YU Shucheng received his BS and MS degrees from the School of Information and Communication Engineering, Beijing University of Posts and Telecommunications, China in 2021 and 2024, respectively. His research interests include integrated sensing and communication and wireless communication.

LIU Xiqing (liuxiqing@bupt.edu.cn) received his MS and PhD degrees from Harbin University of Science and Technology, China and Harbin Institute of Technology, China in 2012 and 2017, respectively. Currently, he is an associate professor with the State Key Laboratory of Networking and Switching Technology, School of Information and Communication Engineering, Beijing University of Posts and Telecommunications, China. His research interests include integrated sensing and communications, waveform designs for wireless transmission, and multiple access technologies. He has served as a technical editor of *IEEE Wireless communications*.

PENG Mugen received his PhD degree in communication and information systems from Beijing University of Posts and Telecommunications (BUPT), China in 2005. Afterward, he joined BUPT, where he has been the deputy director with the State Key Laboratory of Networking and Switching Technology since 2018. Currently, he is the vice president of BUPT. During 2014, he was also an academic visiting fellow with Princeton University, USA. His research interests include integrated sensing and communication, wireless communication theory, and radio signal processing. He was a recipient of the 2018 Heinrich Hertz Prize Paper Award, the 2014 IEEE ComSoc AP Outstanding Young Researcher Award, the Best Paper Award in the ICC 2024 and ICC 2022, etc. He is currently on the Editorial/Associate Editorial Board of the *IEEE Network*, *IEEE Internet of Things Journal*, *IEEE Transactions on Vehicular Technology*, *IEEE Transactions on Network Science and Engineering*, etc.